

## Investigation of metal–insulator-like transition through the *ab initio* density matrix renormalization group approach

E. Fertitta,<sup>1</sup> B. Paulus,<sup>1</sup> G. Barcza,<sup>2</sup> and Ö. Legeza<sup>2</sup><sup>1</sup>*Institut für Chemie und Biochemie, Freie Universität Berlin, Takustraße 3, 14195 Berlin, Germany*<sup>2</sup>*Strongly Correlated Systems “Lendület” Research Group, Wigner Research Centre for Physics, P.O. Box 49, H-1525 Budapest, Hungary*

(Received 9 July 2014; revised manuscript received 27 October 2014; published 18 December 2014)

We have studied the metal–insulator-like transition in pseudo-one-dimensional systems, i.e., lithium and beryllium rings, through the *ab initio* density matrix renormalization group (DMRG) method. Performing accurate calculations for different interatomic distances and using quantum information theory, we investigated the changes occurring in the wave function between a metallic-like state and an insulating state built from free atoms. We also discuss entanglement and relevant excitations among the molecular orbitals in the Li and Be rings and show that the transition bond length can be detected using orbital entropy functions. Also, the effect of different orbital bases on the effectiveness of the DMRG procedure is analyzed comparing the convergence behavior.

DOI: [10.1103/PhysRevB.90.245129](https://doi.org/10.1103/PhysRevB.90.245129)

PACS number(s): 03.65.–w, 03.67.–a, 71.15.–m, 74.20.Pq

### I. INTRODUCTION

We present a metal-insulator transition (MIT) [1–5] investigation in pseudo-one-dimensional systems, i.e., lithium and beryllium rings, through the *ab initio* density matrix renormalization group (DMRG) [6,7]. Despite the apparent simplicity of these model systems, a meaningful description of the transition from the metallic to the insulating regime, i.e., till the dissociation in atomic species, reveals a high complexity due to strong correlation effects which are hard to be described using traditional multiconfigurational approaches. This brought us to choose such a high accuracy wave function method as DMRG. The interest toward these model systems was due to their particular suitability to simulate the behavior of many-level Hubbard models within a quantum chemical (QC) framework through the use of local functions, offering, of course, a bridge between QC and physical model Hamiltonian results. The Hubbard model provides us a minimal model to study MIT as a function of the on-site Coulomb interaction  $U$  and the electron hopping amplitude  $t$ . The corresponding Hamiltonian is written as

$$\mathcal{H} = -t \sum_{i,\sigma} (c_{i\sigma}^\dagger c_{i+1\sigma} + c_{i+1\sigma}^\dagger c_{i\sigma}) + \frac{U}{2} \sum_{\substack{i,\sigma,\sigma' \\ \sigma \neq \sigma'}} n_{i\sigma} n_{i\sigma'}, \quad (1)$$

where  $i$  runs over the  $N$  sites in the chain. The operator  $c_{i\sigma}^\dagger$  ( $c_{i\sigma}$ ) creates (annihilates) an electron at site  $i$  with spin  $\sigma$ , where the spin index is allowed to take on two different values corresponding to the spin-up and spin-down states. Here  $n_{i\sigma}$  denotes the particle-number operator,  $t$  the hopping integral between nearest-neighbor sites, and  $U$  the strength of the on-site Coulomb repulsion. Extension of the model including long-range Coulomb interactions is also known [8–20]. In contrast to this, in our work we study the full *ab initio* Hamiltonian in which the hopping and Coulomb matrix elements are not restricted to nearest neighbors only; thus the general form of the Hamiltonian is given as

$$\mathcal{H} = \sum_{i,j,\sigma} T_{ij} c_{i\sigma}^\dagger c_{j\sigma} + \sum_{\substack{i,j,k,l \\ \sigma,\sigma'}} V_{ijkl} c_{i\sigma}^\dagger c_{j\sigma}^\dagger c_{k\sigma'} c_{l\sigma}. \quad (2)$$

The matrix elements  $T_{ij}$  and  $V_{ijkl}$  are expressed in a molecular orbital (MO) basis obtained by the complete active space self-consistent field (CAS-SCF) method [21] using the MOLPRO quantum chemistry package [22]. The schematic plot of the standard Hubbard model with short-range hopping and on-site Coulomb interaction and the multilevel Hubbard-like model with long-range hopping and delocalized Coulomb interactions are shown in Fig. 1. Therefore, besides modeling the Hubbard system with a Li ring using only  $s$  functions, we can study the effect of the  $p$  orbital basis on the MIT. For such a multiorbital Hubbard-like model, our work serves as an entanglement-based analysis for an *ab initio*-like description of MIT.

In such a transition, the character of the wave function varies dramatically which is reflected by the change of the electron correlation from predominantly dynamic correlation in the metallic case to static correlation in the dissociation limit. This can be analyzed using quantum information theory (QIT), in particular studying the change in orbital entanglement. Indeed, besides reaching energies comparable to the full configuration interaction (CI), DMRG gives us the chance to calculate important quantities such as the one-site entropy [23] and the two-site mutual information [24–28], and the block entropy [23,29,30]. In this work we show how these can be employed to analyze the MIT and identify the position of the transition. Moreover since DMRG allows us to study relatively large systems with high accuracy, we will investigate the size dependence of such properties in order to evaluate the behavior at the thermodynamical limit.

Finally, in the present work we also investigate the effect of the orbital basis on the DMRG results. Although several DMRG works can be found in the literature where various orbital bases were employed to study quantum chemical systems [25–28,31–38], no rigorous analysis in terms of resulting entanglement patterns has been carried out, yet. As we will show, the use of a different basis as well as the starting Hartree-Fock configuration can have a huge impact on the effectiveness of the method. Indeed, despite that in all cases the results converge toward the full-CI limit, we can observe how the choice of a local orbital basis instead of a canonical orbital basis might help to reach that level with less computational effort.

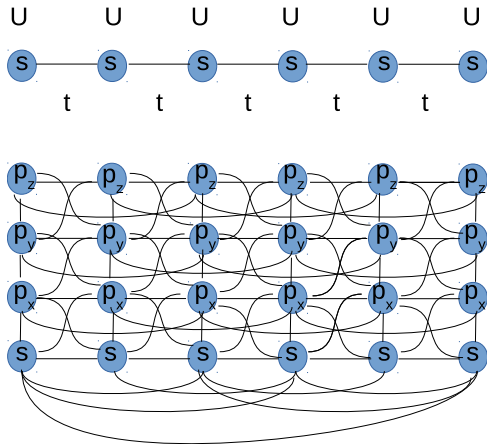


FIG. 1. (Color online) Schematic representation of the standard Hubbard model with short-range hopping interaction and on-site Coulomb interaction (top) and the multilevel Hubbard-like model with long-range hopping and delocalized Coulomb interactions (bottom). Letters  $s$ ,  $p_x$ ,  $p_y$ , and  $p_z$  label the atomic orbital basis. Solid lines indicate long-range interactions among the various orbitals, but due to visibility reasons not all of them are included.

## II. NUMERICAL PROCEDURES

### A. Basis states

As previously mentioned, we focused our interest on the use of different orbital bases to expand the Hilbert space and we investigated their effect on the effectiveness of the DMRG calculations. Indeed, even though, in principle, the same result will be obtained using different orbital bases constructed from the same atomic basis set, the quantum entanglement, which is crucial in the DMRG routine, strongly depends on this choice. The orbital basis that we considered was the canonical orbitals, used to describe the Hartree-Fock (HF) wave function, and the localized orbitals (LOs) obtained from a possible unitary transformation of this basis.

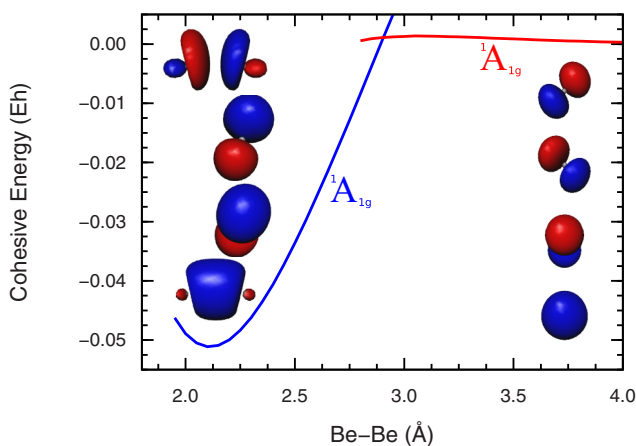


FIG. 2. (Color online) Hartree-Fock ground state potential energy curves calculated for  $\text{Be}_{10}$  determined with the two leading configurations. Additionally the valence and virtual localized orbitals are shown for the two configurations, obtained by a unitary transformation of the corresponding canonical orbital basis.

As sketched in Fig. 2, in the case of beryllium rings two main HF configurations are important, depending on the distance regime, in order to describe the potential energy surface (PES) till dissociation. Around the minimum, the Hartree-Fock wave function presents a high- $p$  character while at larger distances, the HF configuration consists of doubly occupied linear combinations of (almost) pure  $2s$  orbitals. We will refer to these as configurations 1 and 2, respectively. In the two cases, the orbital localization will then yield different LOs. In the first case  $\sigma$ -like orbitals with an  $sp$  character will emerge, while from configuration 2, one will obtain atom-like  $2s$  and  $2p$  bases (see Fig. 2).

In order to describe lithium rings, we also used a local orbital basis. In this case, the occupied LOs were obtained using not only the  $n/2$  doubly occupied valence orbitals, but also the first  $n/2$  virtual orbitals with a mainly  $s$  character. The starting occupation for each LO was then set to 1.

Hartree-Fock calculations, the Foster-Boys localization procedure [39], and generation of integral files for DMRG calculations were all performed using the MOLPRO quantum chemistry package [22]. The atomic basis sets employed consisted of  $1s$ ,  $2s$ , and  $2p$  functions only, and  $1s$  orbitals were always kept frozen. In particular an STO-3G was used for lithium [40] while for beryllium we employed a basis set relying on  $cc$ -pVDZ [41] where only two contracted  $s$  functions and one contracted radial  $p$  function were used.

### B. Density matrix renormalization group method

In order to study the rings built from Li and Be atoms we have employed the quantum chemical version [42] of the density matrix renormalization group (DMRG) method [6,7]. In the past decade this method has been proved to be a rival to the conventional multiconfiguration wave function approaches and nowadays it allows us to study much larger CAS configurations than conventional methods. In our numerical procedure we also utilize various concepts inherited from quantum information theory (QIT) [23,25,26,29,43] which allows us to use DMRG as a black box method [26–28]. In the QC-DMRG applications, the electron-electron correlation is taken into account by an iterative procedure that minimizes the Rayleigh quotient corresponding to the Hamiltonian of the system. For more detailed derivations we refer to the original papers and review articles [42,44–47].

The amount of contribution to the total correlation energy of an orbital can be detected by the single-orbital von Neumann entropy,  $s(1)_i = -\text{Tr} \rho_i \ln \rho_i$ , where  $\rho_i$  is the reduced density matrix at orbital  $i$ . The two-orbital von Neumann entropy is constructed similarly using the reduced density matrix  $\rho_{ij}$  of a subsystem built from orbitals  $i$  and  $j$  and the mutual information  $I_{ij} = s(2)_{ij} - s(1)_i - s(1)_j$  describes how orbitals are entangled with each other as they are embedded in the whole system. The block von Neumann entropy of segments of length  $l = 1, \dots, N - 1$  of the finite chain can be used to study critical and gapped phases where reduced density matrices  $\rho_l$  are generated automatically by the DMRG procedure. For more detailed derivations we refer to the original papers [23,25,26,28–30,43]. Therefore, these quantities provide chemical information about the system,

especially about bond formation and the nature of static and dynamic correlation [27,28,37,48].

In order to use QC-DMRG as a black box method one has to carry out a few optimization steps. First, the arrangement of orbitals along a one-dimensional topology has to be optimized (ordering) in order to reduce the set of Schmidt ranks when the system is systematically partitioned into a left and right parts during the DMRG sweeping procedure [23]. This allows us to carry out calculations with a much smaller number of block states using the dynamical block state selection (DBSS) approach [43,49]. This is achieved by minimizing the entanglement distance, expressed as a cost function,  $\hat{I}_{\text{dist}} = \sum_{i,j} I_{ij} |i - j|^\eta$ , where the entanglement between pairs of orbitals is weighted by the distance in the chain between the orbitals. Using  $\eta = 2$  has the advantage that this optimization task can be carried out using concepts of spectral graph theory [50]. It follows that the so called Fiedler vector  $x = (x_1, \dots, x_N)$  is the solution that minimizes  $F(x) = x^\dagger L x = \sum_{i,j} I_{ij} (x_i - x_j)^2$  subject to the following constraints that  $\sum_i x_i = 0$  and  $\sum_i x_i^2 = 1$ , where the graph Laplacian is  $L_{ij} = D_{ij} - I_{ij}$  with  $D_{ii} = \sum_j I_{ij}$ . The second eigenvector of the Laplacian is the Fiedler vector [51,52] which defines a (1-dimensional) embedding of the graph on a line that tries to respect the highest entries of  $I_{ij}$  and the edge length of the graph. Ordering the entries of the Fiedler vector by a nondecreasing or nonincreasing way provides us a possible ordering. Usually the best ordering does not strongly depend on the number of block states employed; thus this optimization task can be performed efficiently with a preliminary prompt calculation.

Another optimization task is performed in order to speed up the warm-up sweep of the DMRG procedure. Therefore, in order to achieve fast and stable convergence we also utilize the configuration interaction based on a dynamically extended active space (CI-DEAS) procedure [23,26,53]. In this method the active space is expanded iteratively using orbitals with the largest one-orbital entropy values. The sequence by which orbitals are taken into account is determined by the so called CAS vector which is simply a rendered sequence of orbital indices with decreasing one-orbital value.

Therefore, our black-box QC-DMRG is composed of two phases: the *preprocessing phase* in which the ordering and CAS vector are optimized using fixed small number of block states and the *production phase* in which an accurate calculation is performed using the DBSS procedure in order to reach an *a priori* set error margin. In the preprocessing phase, we first use the ordering for which the integral files were generated and a random CAS vector using  $M = 64$  block states. We calculate the one-orbital entropy from which we obtain the CAS vector and we also determine the two-orbital mutual information and the optimal ordering by calculating the Fiedler vector. Next a DMRG calculation is carried out with the optimized ordering and CAS vector and the whole cycle is repeated until we obtain lower total energy. In the next step this procedure is repeated, but with  $M = 256$  states. In the present study, we have performed the accurate calculations in the production phase using the the DBSS procedure with an *a priori* set value of quantum information loss  $\chi = 10^{-4}$  in each DMRG renormalization and truncation step and using a minimum number of block states  $M_{\text{min}} = 512$ . The

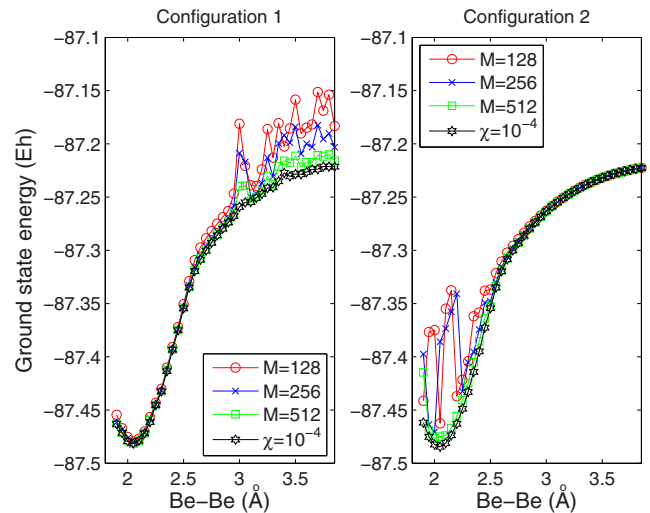


FIG. 3. (Color online) Ground state energy of  $\text{Be}_6$  as a function of Be-Be distance for various fixed number of block states,  $M$ , and for  $\chi = 10^{-4}$  using configuration 1 (left) and configuration 2 (right) and localized orbital basis.

preprocessing phase takes only a small fraction of the total computational time.

In Fig. 3 we show results for  $\text{Be}_6$  using configuration 1 and configuration 2. It is clear that the accuracy of DMRG fluctuates strongly as a function of Be-Be distance when the number of block states is kept fixed while the error can be controlled very efficiently using the DBSS approach.

Finally, we want to underline that, since the mutual information is orbital basis dependent, besides orbital ordering, the entanglement distance  $I_{\text{dist}}$  can be manipulated by changing the orbital basis. Therefore, performance of QC-DMRG can be optimized by using proper choice of the orbital basis; i.e., the same state can be obtained with a much smaller number of block states [54]. Our entanglement analysis can be used in this respect as well, as will be shown below.

### C. Dependence of entanglement on orbital basis and ordering

In this section we report data obtained for  $\text{Be}_6$  using  $M = 512$  block states. Both configurations were employed and a comparison between local and canonical orbital basis is shown. As expected, regardless of the chosen orbital basis, DMRG reaches the same state, but some choices can bring better results. This depends of course on the entanglement of the orbitals in the different situations.

Let us consider the dissociation limit first. Both in canonical and local description we have different sets of many degenerate orbitals, but while the degenerate canonical orbitals, which are delocalized over the whole system, are highly entangled, the localized functions sitting on different centers present a low correlation between each other. Moreover, as could be expected, the LOs derived by configuration 2 converge more effectively in this range.

As an example, the two-orbital mutual information and the one-orbital entropy using the Fiedler vector based ordering optimization are shown in Fig. 4 (left panels) for the ground state of  $\text{Be}_6$  in the insulating regime,  $d = 3.30$  Å, with

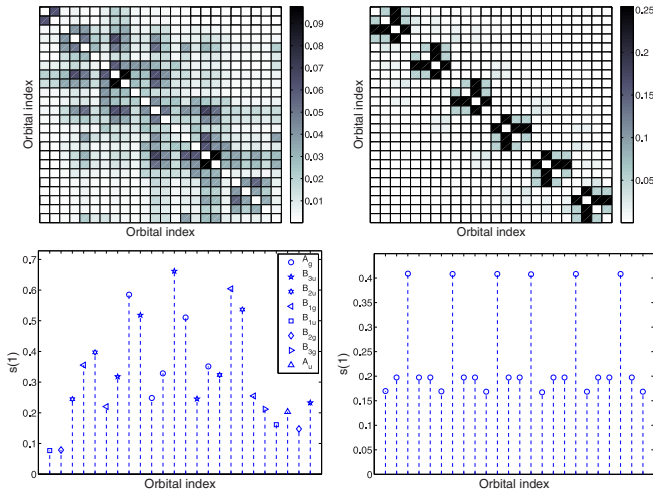


FIG. 4. (Color online) Orbital ordering optimization using the Fiedler vector for the ground state for  $\text{Be}_6$  for a stretched structure,  $d_{\text{Be-Be}} = 3.30 \text{ \AA}$ , using the DMRG method with canonical (left) and local (right) orbitals using configuration 2. Color-scaled plot of two-orbital mutual information (upper) and single-orbital entropy profile (lower).  $I_{\text{tot}} = 7.81, I_{\text{dist}} = 332.38$  with the canonical basis and  $I_{\text{tot}} = 5.83, I_{\text{dist}} = 58.1$  with the local basis.

canonical orbitals and configuration 2. The same are plotted for the case where localized orbitals are used in the right panels. It is evident from the figure that the two-orbital mutual information is more diagonally dominant when localized orbitals were used, and  $I_{\text{dist}}$  dropped from 332 (canonical orbitals) to 58 (localized orbitals). This of course has a tremendous effect on the performance of DMRG since for canonical orbitals the number of required block states to reach the *a priori* set error margin  $\chi = 10^{-3}$  has reached  $M = 3000$  while for localized orbitals it did not grow above  $M = 512$ . It is also remarkable to note that the ordering provided by the Fiedler vector satisfies all intrinsic demands for DMRG with open boundary condition (OBC). Although the  $\text{Be}_6$  ring is a rotationally invariant system, the orbitals of Be atoms are arranged along the 1D chainlike order in a way that the one-orbital entropy profile has a left-right symmetry (see lower-right panel in Fig. 4) and there is no coupling between its two ends. Such configuration is the best choice for DMRG with OBC.

On the other side, in the metallic state, the situation is inverted since the canonical orbitals are distributed in larger energy range and only some of them present a high orbital entropy and are important for the construction of configurations with higher weight. This does not happen if local functions are used, since all of them have important weight. Nevertheless with a proper choice of ordering and block states the local orbitals offer a valid choice of orbital basis for any structure. As an example, we report results using configuration 1 for the equilibrium structure in Fig. 5 for the canonical (left panels) and localized orbitals (right panels), respectively. In this case,  $I_{\text{dist}}$  is again reduced when localized orbitals were used but with a much smaller rate. The optimal ordering provided by the Fiedler vector again gives a symmetric one-orbital entropy distribution and the couplings

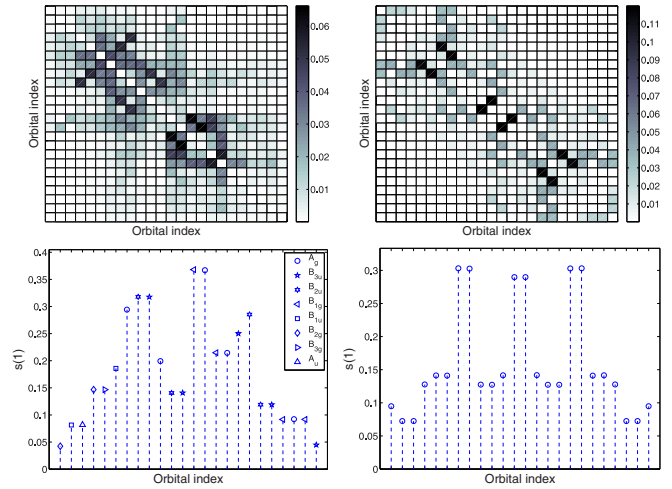


FIG. 5. (Color online) Orbital ordering optimization using the Fiedler vector for the ground state for  $\text{Be}_6$  close to the equilibrium structure,  $d_{\text{Be-Be}} = 2.15 \text{ \AA}$ , using the DMRG method with canonical (left) and local (right) orbitals using configuration 1. Color-scaled plot of two-orbital mutual information (upper) and single-orbital entropy profile (lower).  $I_{\text{tot}} = 4.35, I_{\text{dist}} = 149.70$  with the canonical basis and  $I_{\text{tot}} = 3.88, I_{\text{dist}} = 100.38$  with the local basis.

between the two ends of the chain are minimized. Using the DBSS approach a slightly larger number of block states was needed to reach the same accuracy threshold using canonical orbitals but the difference was much less significant than for the insulating case.

After showing a comparison between canonical and local orbital basis within the DMRG approach, we want to analyze the behavior of the same localized orbitals for different interatomic distances. In Fig. 6 we report mutual information and one-orbital entropy for  $\text{Be}_6$  close to the ground state minimum and using configuration 2. It is important to remember that this starting HF configuration is not an ideal starting point for this structure, but DMRG yields the same state whatever basis is employed. Nevertheless this choice has a tremendous effect on the entanglement and then on the efficiency of the method. In this case, functions on different orbitals are more correlated than orbitals on the same orbitals while, as stated above, using the same configuration for the insulating state only orbitals

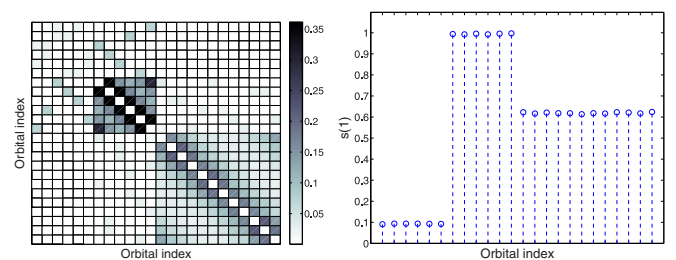


FIG. 6. (Color online) Orbital ordering optimization using the Fiedler vector for the ground state for  $\text{Be}_6$  close to the equilibrium structure,  $d_{\text{Be-Be}} = 2.15 \text{ \AA}$ , using the DMRG method with local orbitals using configuration 2. Color-scaled plot of two-orbital mutual information (left) and single-orbital entropy profile (right).  $I_{\text{tot}} = 13.9, I_{\text{dist}} = 365.58$ .

sitting on the same Be atom are highly entangled. As one can see, comparing Figs. 4 and 6, the mutual information has a block diagonal form for the optimized ordering for both structure, but these represent a totally different situation. At interatomic distance  $d = 2.15 \text{ \AA}$  we find three blocks: in the first block  $2p_z$  orbitals of all Be atoms are grouped; the second block is formed from the  $2p_x$  and  $2p_y$  orbitals of the Be atoms, while the third block is composed from the  $2s$  orbitals of the Be atoms. In contrast to this, for  $d = 3.30 \text{ \AA}$  we find six blocks, each formed by the  $2s$ ,  $2p_x$ ,  $2p_y$ , and  $2p_z$  of a given Be atom. This is very similar to what is observed for lithium, since it shows how close to the minimum the wave function is highly delocalized, while the more the structure is stretched the more it can be described as a state product of orbitals of the individual atoms.

If we now consider configuration 1 once again, we observe in Fig. 5 (upper right) three groups of orbitals with the same orbital entropy which one can easily identify as the valence  $\sigma$ -like orbitals, the  $2p_z$  functions, and the remaining virtual orbitals. The first group present the highest orbital entropy since they are the doubly occupied orbitals of the starting Hartree-Fock configuration.

### III. ENTANGLEMENT ANALYSIS

The energy is not the only interesting result that can be achieved from DMRG calculations. The entanglement pictures used to optimize the DMRG procedure can also be used to extract information about the system. In this section we show entanglement analysis using localized orbitals for the Li and Be rings. This information can be exploited to learn something about the evolution of the wave function along the PES.

In addition, as has been shown in Ref. [55], one can also analyze the sources of entanglement encoded in  $I_{ij}$  by studying the behavior of the matrix elements  $\rho_{ij}$ . These are expressed as the expectation values of *generalized correlation functions*  $\langle \Psi | \mathcal{T}_i^{(m)} \mathcal{T}_j^{(n)} | \Psi \rangle$  where the transition operator  $\mathcal{T}_i^{(m)}$  with  $m = 1, \dots, 16$  describes a possible transition between the four initial,  $|\alpha\rangle$ , and four final states,  $|\alpha'\rangle$ , of orbital  $i$ . Therefore,  $\mathcal{T}^{(m)}$  transforms the state  $|\alpha\rangle$  with  $\alpha = (m-1) \pmod{4}$  into state  $|\alpha'\rangle$  with  $\alpha' = \lfloor (m-1)/4 \rfloor + 1$ ,  $\mathcal{T}^{(m)}|\alpha\rangle = |\alpha'\rangle$ , where  $\lfloor x \rfloor$  denotes the floor function, the integral part of  $x$ . A given generalized correlation function measures the expectation value of the resonance amplitude between the initial and final states within a particular environment and can be expressed as  $\langle \mathcal{T}_i^{(m)} \mathcal{T}_j^{(n)} \rangle = \sum_{\beta} C_{l(m),l(n),\beta}^* C_{r(m),r(n),\beta}$ , where  $r(m) = (m-1) \pmod{q}$  and  $l(m) = \lfloor (m-1)/q \rfloor + 1$ . Here the wave function of the tripartite system is written as  $|\Psi\rangle = \sum_{\alpha_i, \alpha_j, \beta} C_{\alpha_i, \alpha_j, \beta} |\alpha_i, \alpha_j, \beta\rangle$ , where  $\alpha_i$  and  $\alpha_j$  label the bases of the orbitals  $i$  and  $j$ , and  $\beta$  labels the basis of the environment, which is composed of the remaining orbitals. In general,  $\langle \mathcal{T}_i^{(m)} \mathcal{T}_j^{(n)} \rangle$  contains both connected and disconnected contributions between subsystems  $i$  and  $j$ . In order to circumvent this behavior, we generally study the connected part of the generalized correlation functions,  $\langle \mathcal{T}_i^{(m)} \mathcal{T}_j^{(n)} \rangle_C = \langle \mathcal{T}_i^{(m)} \mathcal{T}_j^{(n)} \rangle - \langle \mathcal{T}_i^{(m)} \rangle \langle \mathcal{T}_j^{(n)} \rangle$ , where the disconnected part, given by the product of the expectation values of the local transition operators, is subtracted out. Note that the mutual information is formulated in such a way that the

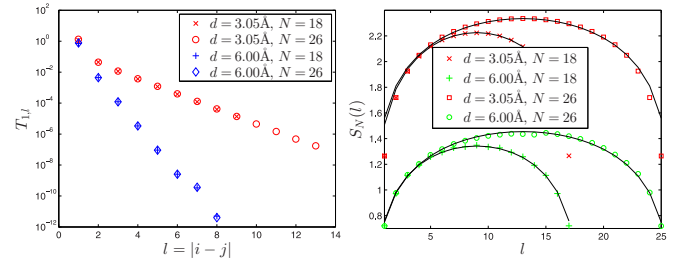


FIG. 7. (Color online) Decay of the hopping matrix elements as a function of  $l$ th-neighbor distance for a ring cluster built from 18 and 26 Li atoms calculated using only  $2s$  functions for bond length  $d_{\text{Li-Li}} = 3.05 \text{ \AA}$  and for  $d_{\text{Li-Li}} = 6.00 \text{ \AA}$  (left). Length dependence of the von Neumann entropy of segments of length  $l = 1, \dots, N-1$  of the finite chain (right). The solid lines are our fit using Eq. (3).

disconnected parts of the generalized correlation functions do not contribute. As we will see below, these can be used to identify the relevant physical processes that lead to the generation of the entanglement.

#### A. Li rings with only $2s$ functions

Despite that  $p$  functions are fundamental for a fair description of the chemistry of lithium, we can learn important information about the physics of correlated electrons in metallic systems using only  $2s$  atomic orbitals for Li rings. Using a localized orbital basis to describe such a system through any *ab initio* method is analogous to a Hubbard model with long-range interactions and with one function per site. In this sense stretching the bond length in the lithium rings is equivalent to change  $t$  and so the  $U/t$  of a half-filled Hubbard model. As an example, in the left panel of Fig. 7 we show the hopping matrix elements as a function of  $l$ th-neighbor distance for the metallic regime at  $d_{\text{Li-Li}} = 3.05 \text{ \AA}$  and for the insulating regime at  $d_{\text{Li-Li}} = 6.00 \text{ \AA}$  for Li rings consisting of 18 and 26 atoms. It is clearly seen that in the metallic regime the hopping falls off significantly slower than in the insulating regime.

As expected and independently on the size of the system, all localized orbitals have the same site entropy respecting the rotational invariance of the system. The way these values change with the structure resembles what one can observe in a Hubbard model. In the metallic case the delocalization of the  $n$  electrons in  $n$  equivalent orbitals leads to the conclusion that the four possibilities (empty, up-spin, down-spin, and doubly occupied) have the same weight for each orbital ( $1/4$ ), from which  $s(1) = \ln 4 = 1.386$ . The calculated eigenvalues of the one-orbital reduced density matrix for a finite ring with  $N = 26$  are  $\omega_0 = 0.13, \omega_{\downarrow} = 0.37, \omega_{\uparrow} = 0.37$ , and  $\omega_{\downarrow\uparrow} = 0.13$  corresponding to the empty, down-spin, up-spin, and doubly filled basis states. It follows that the orbital entropy is  $s(1) = 1.266$  which indicates that all four basis states gain finite weight, being a clear sign of a metallic behavior analogous to the Hubbard model at small Hubbard  $U$ . Note that in the half-filled Hubbard model a finite gap opens in the charge sector for arbitrary small  $U > 0$  value [3]. The corresponding block entropy profile is shown in the right panel of Fig. 7. The central charge  $c$  can be derived [30] from the

initial slope of the length dependence of  $s_N(l)$

$$s_N(l) = \frac{c}{3} \ln \left[ \frac{N}{\pi} \sin \left( \frac{\pi l}{N} \right) \right] + c'_1, \quad (3)$$

where  $c'_1$  is a nonuniversal constant. On the other hand for noncritical, gapped models,  $s_N(l)$  saturates to a finite value when  $l$  is far from the boundaries. Our fits using Eq. (3) yielding central charge values  $c = 1.23$  and  $c = 1.10$  for  $N = 18$  and  $N = 26$ , respectively, are indicated by solid lines. In order to gain more insight about the metallic phase, we have also calculated the spin gap,  $\Delta_s$ , and charge gap,  $\Delta_c$ , defined as

$$\Delta_s(N) = E(N/2 + 1, N/2 - 1) - E(N/2, N/2), \quad (4)$$

$$\Delta_c(N) = E(N/2 + 1, N/2) + E(N/2 - 1, N/2) - 2E(N/2, N/2), \quad (5)$$

where  $E(N_\uparrow, N_\downarrow)$  stands for the ground state energy obtained for the finite system with  $N_\uparrow$  electrons with up-spin and  $N_\downarrow$  with down-spins. Although for finite systems finite gaps are expected in all excitation modes we have found that the gaps are very small. The spin gap was found to be  $10^{-4}$  and  $10^{-8} E_h$  for  $N = 18$  and  $26$ , respectively, which leads to  $c = 1$ . On the other hand, the charge gap shows a stronger finite-size dependence. By carrying out finite-size scaling of the charge gap for systems up to 26 sites we have estimated the charge gap to be  $0.09 E_h$  in the thermodynamic limit using a second-order polynomial fit. For an even more compressed geometry, i.e., for  $d = 2.50 \text{ \AA}$ , we obtained  $\Delta_c(N \rightarrow \infty) = 0.045 E_h$ . Since these small values are comparable with the uncertainty arising in the extrapolation procedure from the use of limited-size systems, we will consider them zero. We could not study much longer chains since the generation of the integrals took significantly more time with increasing system size. As a further check by setting all  $V_{ijkl}$  elements to zero we obtained  $c = 2.04$  and  $c = 2.02$  for  $N = 18$  and  $26$ , respectively, in agreement with the expected result for a Hubbard model with  $U = 0$ .

On the other hand, at the dissociation limit the wave function can be described as a state product of  $2s$  orbitals of Li atoms in  $^2S$  states which means that the only possibilities are up-spin and down-spin electrons per each site. This is clearly reflected by the eigenvalues of the one-orbital reduced density matrix obtained for an insulating situation ( $d_{\text{Li-Li}} = 6.00 \text{ \AA}$ ) which are almost zero for the empty and doubly occupied orbital [0.002(1)] and 0.500(4) for up- and down-spin. The orbital entropy  $s(1) = 0.720(2)$  being close to  $\ln 2 = 0.693$  indicates again that only two basis states gain finite weight so the empty and doubly filled basis states are excluded from the wave function. The corresponding block entropy is shown in the right panel of Fig. 7 and our fit yields  $c = 1.03$  and  $c = 1.01$  for  $N = 18$  and  $N = 26$ , respectively. The spin gap was again found to be very small, i.e.,  $10^{-7}$  and  $10^{-10} E_h$  for  $N = 18$  and  $N = 26$ , respectively. In contrast to the metallic case, the charge gap basically showed no finite-size dependence in the insulating phase and for all system sizes from  $N = 6$  to  $26$  we obtained a finite value of  $\Delta_c = 0.18 E_h$  and  $\Delta_c = 0.26 E_h$ , for  $d_{\text{Li-Li}} = 4.00 \text{ \AA}$  and  $d_{\text{Li-Li}} = 6.00 \text{ \AA}$ , respectively. Increasing the interatomic distance even further we obtained  $\Delta_c = 0.28 E_h$  for  $d_{\text{Li-Li}} = 12.00 \text{ \AA}$ . Therefore, the finite charge gap

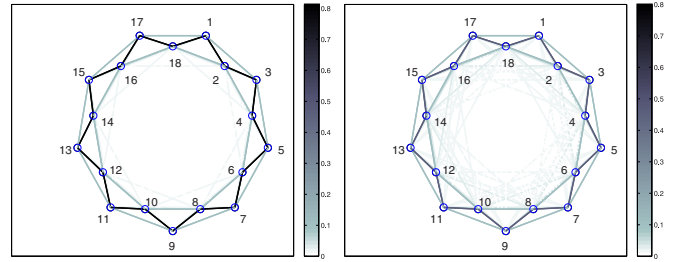


FIG. 8. (Color online) Schematic plot of the two-orbital mutual information for a ring cluster built from 18 Li atoms but using only  $2s$  functions of the Li atoms for bond length  $d_{\text{Li-Li}} = 3.05 \text{ \AA}$  (left) and for  $d_{\text{Li-Li}} = 6.00 \text{ \AA}$  (right).

and the obtained value of  $c = 1$  for the central charge together resemble the characteristics of an insulating phase.

Let us now consider the two-orbital mutual information. In Fig. 8 we report its schematic representation for  $\text{Li}_{18}$  in a metallic and insulating regime. In the first case, at interatomic distance  $3.05 \text{ \AA}$ , all orbitals are highly entangled among each other, because of the high delocalization of the wavefunction in this regime. Of course, the value of  $I_{ij}$  reduces if more distant neighbors are considered. We show this decay for both regimes and for  $\text{Li}_{18}$  and  $\text{Li}_{26}$  in Fig. 9 in a log-log plot. As one can see, in the insulating state the linear trend is not affected by the size of the system, while at shorter interatomic distance, the slope of the linear decay increases if going from  $\text{Li}_{18}$  and  $\text{Li}_{26}$ .

It has to be underlined that in the insulating regime, other orbitals are also highly entangled, but the nature of this correlation is totally different than in the previous case. In order to see this, one has to observe the different elements of the two-orbital density matrix shown in Fig. 14 in the Appendix. While in a metallic situation different hopping and spin-flipping terms have a large contribution (left panels), only the spin flipping plays a role in a stretched structure (right panels). This is because even at dissociation the separated atoms present a strong quantum entanglement in the singlet state we are considering. Confirming this is the fact that at the same structure, the almost degenerate state with highest spin multiplicity (ferromagnet state) presents no entanglement among the  $2s$  orbitals, since the wave function can be described as a pure state product.

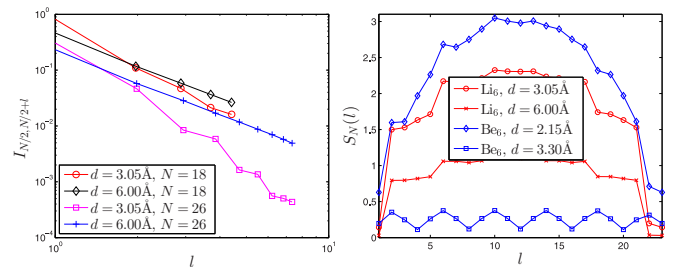


FIG. 9. (Color online) Decay of the  $n$ th-neighbor entanglement bond strength measured as a function of the interatomic distance for the Li ring represented with only  $2s$  orbitals for a metallic state ( $d_{\text{Li-Li}} = 3.05 \text{ \AA}$ ) and for insulating situation at  $d_{\text{Li-Li}} = 6.00 \text{ \AA}$  (left). Block entropy profiles obtained for the  $\text{Li}_6$  and  $\text{Be}_6$  rings for various interatomic distances (right).

**B. Li ring with 2s and 2p functions**

The next step in the study of lithium systems is the analysis of the effect of *p* atomic functions. Because of the obvious increase of the active space we focused our attention on the smaller ring  $\text{Li}_6$ , but the reduced size does not have drastic effects on the nature of the system.

In Fig. 10 the two-orbital mutual information and the one-orbital entropy are reported for both the metallic and the insulating state. The presence of the three *2p* atomic functions per site increases, of course, the complexity of the entanglement picture, but the main information is analogous to what is observed for larger Li rings with *2s* orbitals only. First, once again, independently of the structure, the rotational symmetry is respected in the degeneracy of the one-site entropy values. Moreover, the highest entanglement still occurs among the *2s* orbitals especially at long interatomic distances because of the spin-flipping (see Fig. 13) and the  $s(1)$  are just slightly effected by the presence of *2p* orbitals.

The entanglement between *2s* and *2p* or between *2p* orbitals is an order of magnitude smaller then between *2s* atomic functions and decreases sensibly going from a metallic to an insulating state. This reflects the fact that intraband transitions within the half-filled *2s* band are more important than interband transitions. Moreover we observe that the  $2p_z$  orbitals are only entangled with *2s* orbitals, while the *2p* atomic functions lying in the plane of the ring would seem to be correlated between each other only if centered on the same Li atom. Moreover, comparing the correlation functions reported in Figs. 14 and 13 of the Appendix, one can see that because of the presence of the *2p* orbitals, the hopping terms gain importance also at large interatomic distance.

As expected, toward dissociation the correlation between *s* and *p* orbitals on the same site drops even more. Indeed, one has to remember that in free Li atoms (if core electrons are kept frozen as we did) the correlation energy is zero and the HF wave function with one electron in the *2s* orbital represents

the correct solution within the limit of the atomic basis set. So it is clear that the *s-p* entanglement has to get to zero with increasing distance. In order to gain more insight, we have to consider the block entropy profiles as well. However, since the site entropy is not constant, the block entropy profile depends on the ordering of orbitals along the one-dimensional chain used in the DMRG treatment [23]. In Fig. 9 (right) the block entropy profile is shown for the ordering used in Fig. 10 for the metallic region at  $d_{\text{Li-Li}} = 3.05 \text{ \AA}$  and for the insulating regime at  $d_{\text{Li-Li}} = 6.00 \text{ \AA}$ . It is clearly seen that the block entropy drops significantly for the latter case and the saturation is a clear sign of the finite charge gap.

**C. Be ring**

In this last section we will analyze the results obtained for beryllium rings. For this system, the use of both *2s* and *2p* atomic bases is mandatory to have a minimal meaningful description.

As one can see, observing Figs. 10 and 11, the main differences between  $\text{Be}_6$  and  $\text{Li}_6$ , besides the strong correlation between *2s* and *2p* orbitals, occurs at dissociation. As *2s* orbitals are doubly occupied in the HF solution, hopping and flipping between them are less important than in the case of lithium and the quantum entanglement between isolated Be atoms can be considered zero. On the other hand, the quasidegeneracy of *2s* and *2p* orbitals causes that the static correlation constitutes about 93% of the total correlation energy. This can be deduced by the strong entanglement shown in the pictorial representation of the mutual information. The block entropy profile shown in Fig. 9 (right) drops again significantly by going from the metallic to the insulating regime. In the latter case, besides the saturation of the block entropy, there is an oscillation with a period of 4 and the block entropy drops to almost zero for every fourth data point. This means that the wave function can be constructed from slightly entangled units built from the four highly entangled orbitals

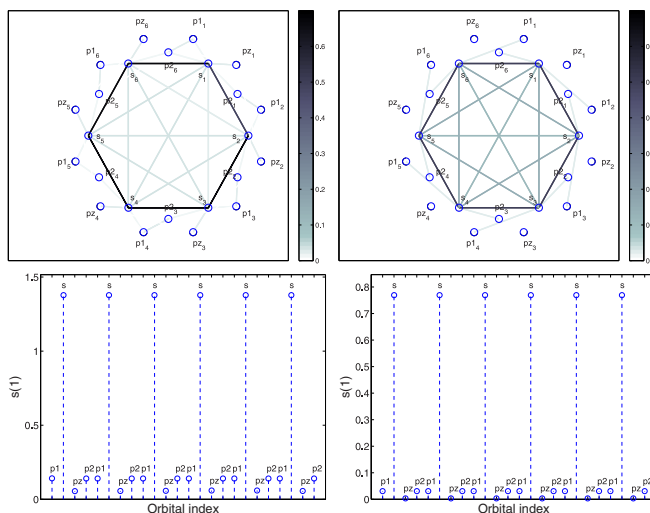


FIG. 10. (Color online) Schematic plot of the two-orbital mutual information (upper panels) and one-orbital entropy (lower panels) for  $\text{Li}_6$  ring calculated using *2s* and *2p* atomic functions for bond lengths  $d_{\text{Li-Li}} = 3.05 \text{ \AA}$  (left) and for  $d_{\text{Li-Li}} = 6.00 \text{ \AA}$  (right).

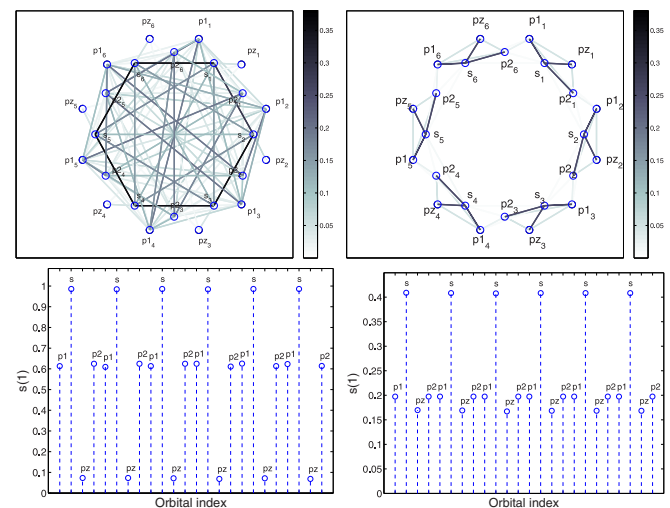


FIG. 11. (Color online) Schematic plot of the two-orbital mutual information (upper panels) and one-orbital entropy (lower panels) for  $\text{Be}_6$  ring calculated using *2s* and *2p* atomic functions for bond lengths  $d_{\text{Be-Be}} = 2.15 \text{ \AA}$  (left) and for  $d_{\text{Be-Be}} = 3.30 \text{ \AA}$  (right) using configuration 2.

of each atom in agreement as was found by studying the one- and two-orbital entropy functions.

Analyzing the correlation functions reported in Fig. 13 of the Appendix, it is evident that in comparison to lithium the hoppings between neighboring  $2p$  atomic functions play a more important role for short interatomic distances. This can be interpreted as an index of a metallic character, since it highlights the delocalized character of the wave function. Despite that from a band structure (i.e., one-electronic) picture, one could conclude that Be rings are insulating, when static correlation is rightfully described, one can observe a metallic-like behavior analyzing indicators other than the band gap.

As already discussed in Ref. [56], the one-orbital entropy function can also be used to locate an avoided crossing. Since a metal-insulator-like transition can be identified as a state transition in finite systems, we can use strong change in  $I_{\text{tot}}$  to identify it. This is a more advanced approach than calculating the low-lying energy spectrum since it requires calculating ground state properties only [24]. Therefore, the behavior of  $I_{\text{tot}}$  as a function of interatomic distance can be used to detect and locate transition points where the wave function changes dramatically. In first panel of Fig. 12 energies of the two lowest-lying  $^1A_g$  singlet states of  $\text{Be}_6$  as a function of  $d_{\text{Be-Be}}$  are shown around the avoided crossing. In the second panel the total quantum information calculated using configuration 1 and 2 is reported. Despite that  $I_{\text{tot}}$  strongly

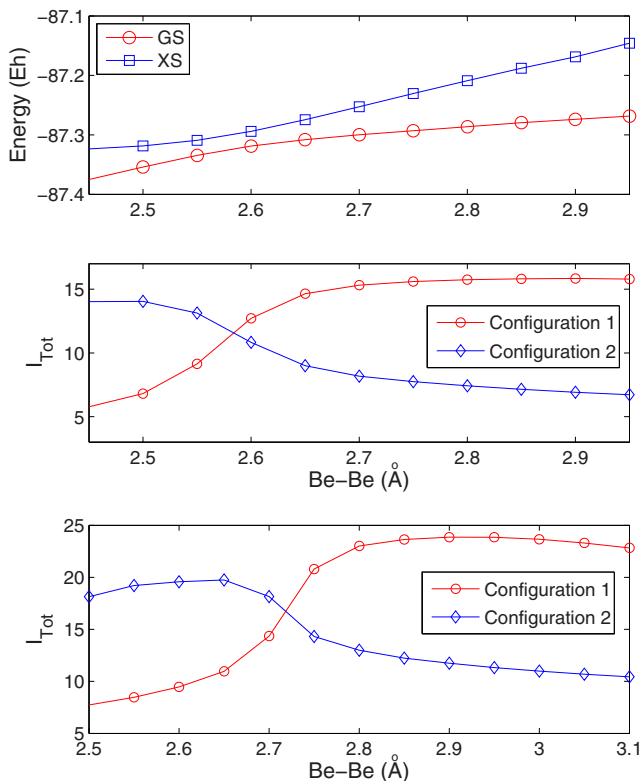


FIG. 12. (Color online) Energies of the two lowest lying  $^1A_g$  singlet states and total quantum information  $I_{\text{tot}}$  for  $\text{Be}_6$  and  $\text{Be}_{10}$  (in this case only  $I_{\text{tot}}$  is considered) as a function of  $d_{\text{Be-Be}}$ , calculated using localized orbitals for configuration 1 and configuration 2. The sudden change in  $I_{\text{tot}}$  indicating the position of the avoided crossing occurs at  $d_{\text{Be-Be}} \simeq 2.55$  Å for  $\text{Be}_6$  and  $2.72$  Å for  $\text{Be}_{10}$ .

depends on the orbital basis employed, it always show strong fluctuations around a state transition, like the one proposed. In our case, we observe how if one configuration or the other is used, a jump or a drop of its value occurs. In both cases this dramatic change occurs at  $d_{\text{Be-Be}} \simeq 2.55$  Å which indicates the position of the avoided crossing. The same observation is true also for the larger cluster  $\text{Be}_{10}$ . As can be seen in the lower panel of Fig. 12, in this case, the avoided crossing can be localized at  $d_{\text{Be-Be}} \simeq 2.70$  Å by studying  $I_{\text{tot}}$ .

#### IV. CONCLUSION

An *ab initio* density matrix renormalization group study has been performed on pseudo-one-dimensional systems in order to investigate the metal-insulator-like transition. Through DMRG we overcame the active space size problem encountered for beryllium rings and we were able to perform very accurate calculations reaching the full-CI level which is generally prohibitive for these systems even with a minimal basis set.

Unlike the Hubbard model which provides us a minimal model to study the MIT as a function of the on-site Coulomb interaction  $U$  and the electron hopping amplitude  $t$  in the full *ab initio* Hamiltonian the hopping and Coulomb matrix elements are not restricted to nearest-neighbors only. The analysis of generalized correlation functions was used to study the change occurring in the wave function as a function of the interatomic distance. Underlying the differences in the entanglement between different orbitals, we showed how the systems evolve from a metallic state to an insulating one. Also through the analysis of the block entropy and energy gaps for lithium rings with  $s$ -like localized basis only, we recovered the Hubbard-like behavior in the two limiting cases. Furthermore we discussed that, despite that the total quantum information strongly depends on the orbital basis, it can be employed to locate the position of the MIT in these systems.

Finally, we focused on the effect of the orbital basis on the DMRG procedure. Comparing the results obtained using canonical and localized orbital bases, we observed that using the latter less computational effort was necessary to reach the same level of accuracy because of the different orbital entanglement which, as discussed, is crucial in quantum chemical DMRG.

#### ACKNOWLEDGMENTS

This research was supported in part by the Hungarian Research Fund (OTKA) under Grants No. NN110360 and No. K100908, the Agence Nationale de la Recherche (ANR), and the German Research Foundation (DFG) via the project “Quantum-chemical investigation of the metal-insulator transition in realistic low-dimensional” (action ANR-11-INTB-1009 MITLOW PA1360/6-1). Financial support by the Max Planck Society is appreciated.

#### APPENDIX

In this appendix we report the pictorial representation of the generalized correlation functions used to construct the off-diagonal elements of the two-orbital reduced density matrix for the different systems analyzed above (see Figs. 13 and 14).

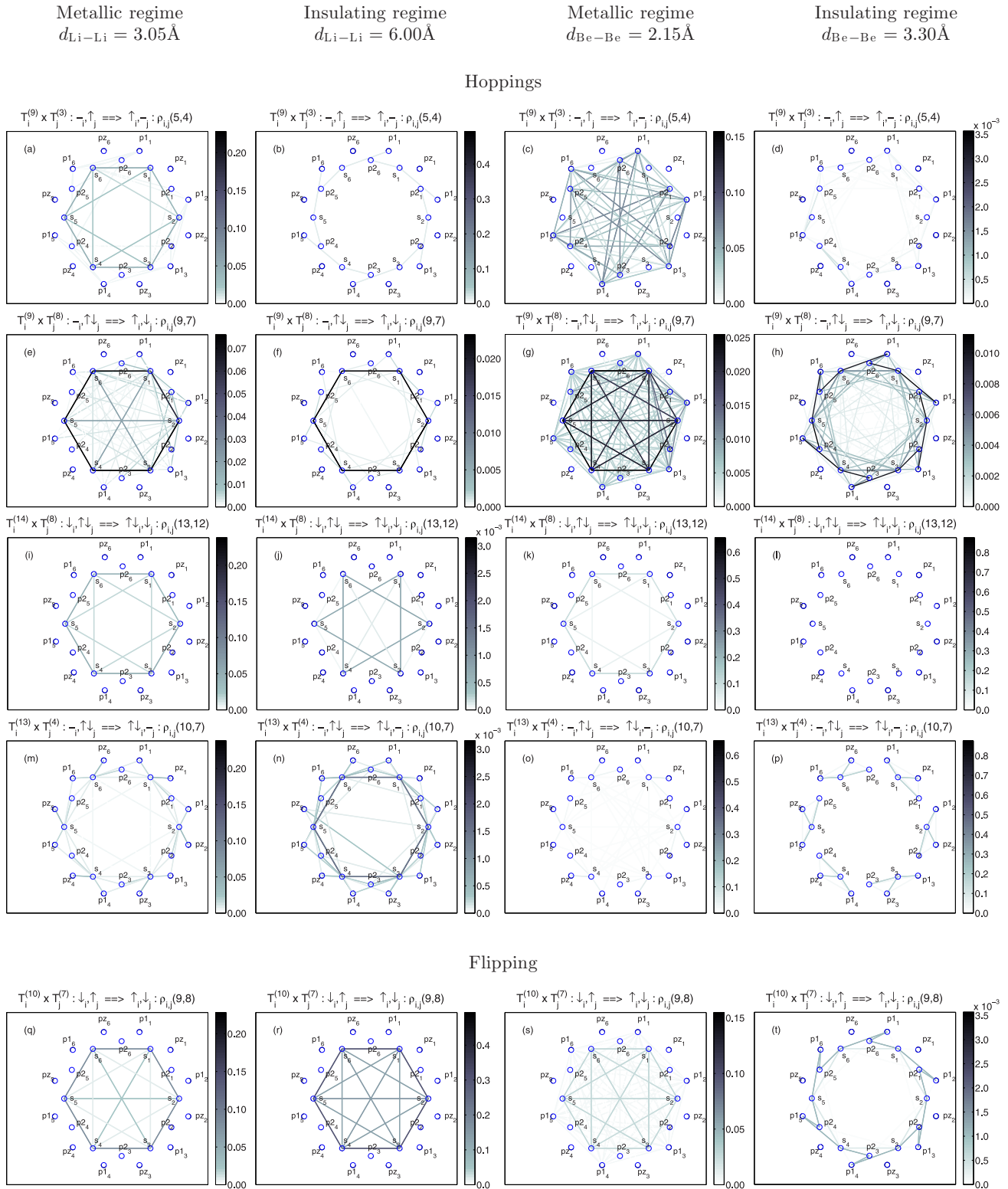
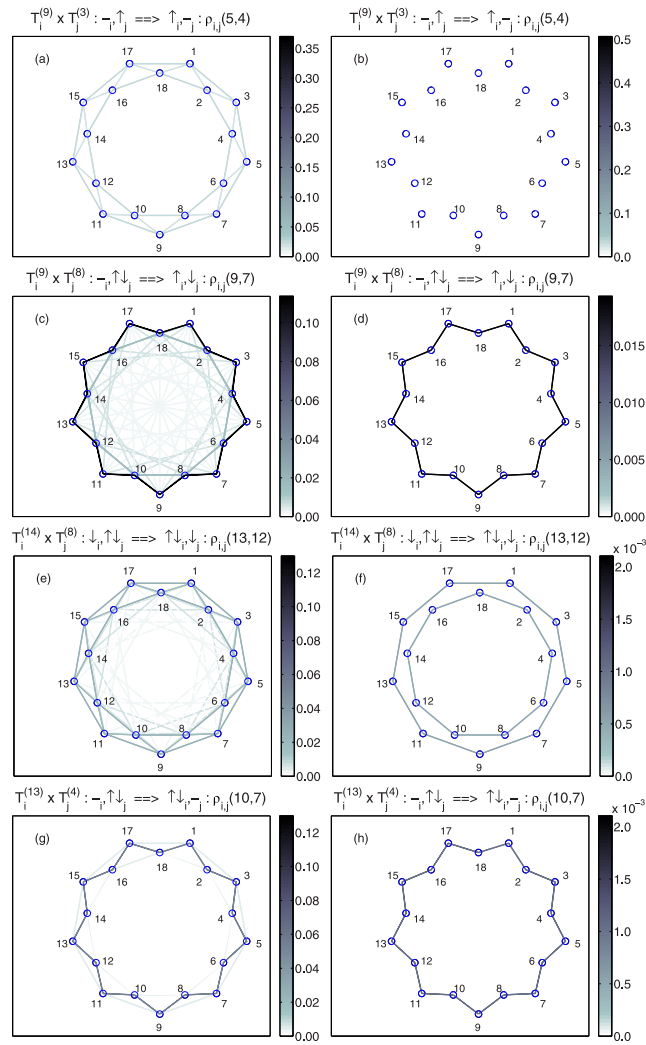


FIG. 13. (Color online) Pictorial representation of the absolute value of the generalized correlation functions used to construct the lower-triangular elements of the two-orbital reduced density matrix for  $Li_6$  and  $Be_6$  using  $2s$  and  $2p$  atomic functions at  $d_{Li-Li} = 3.05 \text{ \AA}$ ,  $d_{Li-Li} = 6.00 \text{ \AA}$ ,  $d_{Be-Be} = 2.15 \text{ \AA}$ , and  $d_{Be-Be} = 3.30 \text{ \AA}$  (from left to right). Strength of transition amplitudes between initial  $(|\alpha_i\rangle|\beta_j\rangle)$  and final states  $(|\alpha'_i\rangle|\beta'_j\rangle)$  on orbital  $i$  and  $j$  are indicated with different line colors. Note the different scales used for color bars in the cases of the various figures.

Metallic regime  
 $d_{Li-Li} = 3.05 \text{ \AA}$

Insulating regime  
 $d_{Li-Li} = 6.00 \text{ \AA}$

Hoppings



Flipping

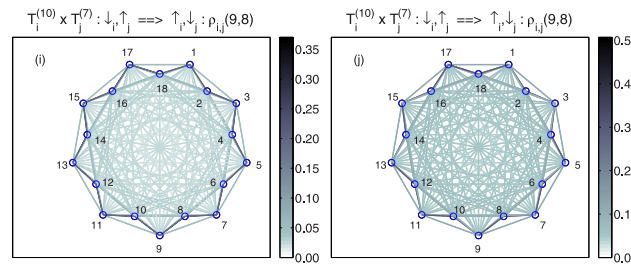


FIG. 14. (Color online) Pictorial representation of the absolute value of the generalized correlation functions used to construct the lower-triangular elements of the two-orbital reduced density matrix for  $Li_{18}$  using only  $2s$  atomic functions at  $d_{Li-Li} = 3.05 \text{ \AA}$  and at  $d_{Li-Li} = 6.00 \text{ \AA}$ . Strength of transition amplitudes between initial  $(|\alpha_i\rangle|\beta_j\rangle)$  and final states  $(|\alpha'_i\rangle|\beta'_j\rangle)$  on orbital  $i$  and  $j$  are indicated with different line colors. Note the different scales used for color bars in the cases of the various figures.

- [1] N. F. Mott, *Rev. Mod. Phys.* **40**, 677 (1968).
- [2] W. Kohn, *Phys. Rev.* **133**, A171 (1964).
- [3] E. Lieb and F. Wu, *Phys. Rev. Lett.* **20**, 1445 (1968).
- [4] M. Imada, A. Fujimori, and Y. Tokura, *Rev. Mod. Phys.* **70**, 1039 (1998).
- [5] R. Resta, *J. Chem. Phys.* **124**, 104104 (2006).
- [6] S. R. White, *Phys. Rev. Lett.* **69**, 2863 (1992).
- [7] S. R. White, *Phys. Rev. B* **48**, 10345 (1993).
- [8] A. Race, W. Barford, and R. J. Bursill, *Phys. Rev. B* **64**, 035208 (2001); **67**, 245202 (2003).
- [9] G. Barcza, W. Barford, F. Gebhard, and Ö. Legeza, *Phys. Rev. B* **87**, 245116 (2013).
- [10] J. Rissler, F. Gebhard, and E. Jeckelmann, *J. Phys. Condens. Matter* **17**, 4093 (2003).
- [11] A. Grage, F. Gebhard, and J. Rissler, *J. Stat. Mech.: Exp. Theor.* (2005) P08009.
- [12] F. Gebhard, *The Mott Metal-Insulator Transition*, Springer Tracts in Modern Physics, Vol. 137 (Springer-Verlag, Berlin, Heidelberg, 1997).
- [13] F. Mila and X. Zotos, *Europhys. Lett.* **24**, 133 (1993).
- [14] K. Penc and F. Mila, *Phys. Rev. B* **49**, 9670 (1994).
- [15] C. Raghunathan, Y. Anusooaya Pati, and S. Ramasesha, *Phys. Rev. B* **65**, 155204 (2002).
- [16] K. Aryanpour, A. Roberts, A. Sandhu, R. Rathore, A. Shukla, and S. Mazumdar, *J. Phys. Chem. C* **118**, 6 (2014).
- [17] K. Aryanpour, A. Shukla, and S. Mazumdar, *J. Chem. Phys.* **140**, 104301 (2014).
- [18] S. Thomas and K. S. Kim, *Phys. Chem. Chem. Phys.* **16**, 24592 (2014).
- [19] S. Sahoo, V. M. L. D. Prasad Goli, S. Ramasesha, and D. Sen, *J. Phys. Condens. Matter* **24**, 115601 (2012).
- [20] C. Mund, O. Legeza, and R. M. Noack, *Phys. Rev. B* **79**, 245130 (2009).
- [21] B. O. Roos and P. R. Taylor, *Chem. Phys.* **48**, 157 (1980).
- [22] H. J. Werner, P. J. Knowles, G. Knizia, F. R. Manby, M. Schütz *et al.*, MOLPRO, Ver. 2012.1, a package of *ab initio* programs, <http://www.molpro.net>.
- [23] Ö. Legeza and J. Sólyom, *Phys. Rev. B* **68**, 195116 (2003).
- [24] Ö. Legeza, and J. Sólyom, *Phys. Rev. Lett.* **96**, 116401 (2006).
- [25] J. Rissler, R. M. Noack, and S. R. White, *Chem. Phys.* **323**, 519 (2006).
- [26] G. Barcza, Ö. Legeza, K. H. Marti, and M. Reiher, *Phys. Rev. A* **83**, 012508 (2011).
- [27] K. Boguslawski, P. Tecmer, Ö. Legeza, and M. Reiher, *J. Phys. Chem. Lett.* **3**, 3129 (2012).
- [28] K. Boguslawski, P. Tecmer, G. Barcza, Ö. Legeza, and M. Reiher, *J. Chem. Theory Comput.* **9**, 2959 (2013).
- [29] G. Vidal, J. I. Latorre, E. Rico, and A. Kitaev, *Phys. Rev. Lett.* **90**, 227902 (2003).
- [30] P. Calabrese and J. Cardy, *J. Stat. Mech.: Theory Exp.* (2004) P06002.
- [31] Ö. Legeza, J. Röder, and B. A. Hess, *Mol. Phys.* **101**, 2019 (2003).
- [32] D. Ghosh, J. Hachmann, T. Yanai, and G. K. L. Chan, *J. Chem. Phys.* **128**, 144117 (2008).
- [33] H. G. Luo, M. P. Qin, and T. Xiang, *Phys. Rev. B* **81**, 235129 (2010).
- [34] A. O. Mitrushchenkov, G. Fano, R. Linguerri, and P. Palmieri, *Int. J. Quant. Chem.* **112**, 1606 (2012).
- [35] Y. Ma and H. Ma, *J. Chem. Phys.* **138**, 224105 (2013).
- [36] S. Wouters, W. Poelmans, P. W. Ayers, and D. Van Neck, *Comput. Phys. Commun.* **185**, 1501 (2014).
- [37] Y. Kurashige, G. K.-L. Chan, and T. Yanai, *Nat. Chem.* **5**, 660 (2013).
- [38] S. Wouters and D. Van Neck, *Eur. Phys. J. D* **68**, 272 (2014).
- [39] M. Foster and S. F. Boys, *Rev. Mod. Phys.* **32**, 296 (1960).
- [40] W. J. Hehre, R. F. Stewart, and J. A. Pople, *J. Chem. Phys.* **51**, 2657 (1969).
- [41] T. H. Dunning, *J. Chem. Phys.* **90**, 1007 (1989).
- [42] S. R. White and R. L. Martin, *J. Chem. Phys.* **110**, 4127 (1999).
- [43] Ö. Legeza, and J. Sólyom, *Phys. Rev. B* **70**, 205118 (2004).
- [44] Ö. Legeza, R. Noack, J. Sólyom, and L. Tincani, in *Computational Many Particle Physics*, edited by H. Fehske, R. Schneider, and A. Weisse, Lecture Notes in Physics, Vol. 739 (Springer, Berlin, 2008), p. 653.
- [45] G. K.-L. Chan and S. Sharma, *Annu. Rev. Phys. Chem.* **62**, 465 (2011).
- [46] K. H. Marti and M. Reiher, *Z. Phys. Chem.* **224**, 583 (2010).
- [47] Y. Kurashige, *Mol. Phys.* **112**, 1485 (2014).
- [48] P. Tecmer, K. Boguslawski, Ö. Legeza, and M. Reiher, *Phys. Chem. Chem. Phys.* **16**, 719 (2014).
- [49] Ö. Legeza, J. Röder, and B. A. Hess, *Phys. Rev. B* **67**, 125114 (2003).
- [50] J. E. Atkins, E. G. Boman, and B. Hendrickson, *SIAM J. Comput.* **28**, 297 (1998).
- [51] M. Fiedler, *Czech. Math. J.* **23**, 298 (1973).
- [52] M. Fiedler, *Czech. Math. J.* **25**, 619 (1975).
- [53] Ö. Legeza and J. Sólyom, International Workshop on “Recent Progress and Prospects in Density-Matrix Renormalization,” Lorentz Center, Leiden University, The Netherlands, <http://www.itp.uni-hannover.de/~jeckelm/dmrg/workshop/proceedings.html>.
- [54] Ö. Legeza, F. Gebhard, and J. Rissler, *Phys. Rev. B* **74**, 195112 (2006).
- [55] G. Barcza, R. M. Noack, J. Sólyom, and Ö. Legeza, [arXiv:1406.6643](https://arxiv.org/abs/1406.6643).
- [56] V. Murg, F. Verstraete, R. Schneider, P. R. Nagy, and Ö. Legeza, [arXiv:1403.0981](https://arxiv.org/abs/1403.0981).